ELSEVIER

Biophysical Chemistry 97 (2002) 213–231

Biophysical Chemistry

www.elsevier.com/locate/bpc

Coherent and robust modulation of a metabolic network by cytoskeletal organization and dynamics

Miguel A. Aon*, Sonia Cortassa

Instituto Tecnológico de Chascomús (INTECH/CONICET), Casilla de Correo 164, 7130- Chascomús, Buenos Aires, Argentina

Received 28 January 2002; received in revised form 12 March 2002; accepted 15 March 2002

Abstract

In order to investigate the influence of cytoskeletal organization and dynamics on cellular biochemistry, a mathematical model was formulated based on our own experimental evidence. The model couples microtubular protein (MTP) dynamics to the glycolytic pathway and its branches: the Krebs cycle, ethanolic fermentation, and the pentose phosphate (PP) pathway. Results show that the flux through glycolysis coherently and coordinately increases or decreases with increased or decreased levels of polymerized MTP, respectively. The rates of individual enzymatic steps and metabolite concentrations change with the polymeric status of MTP throughout the metabolic network. Negative control is exerted by the PP pathway on the glycolytic flux, and the extent of inhibition depends inversely on the polymerization state of MTP, i.e. a high degree of polymerization relieves the negative control. The stability of the model's steady state dynamics for a wide range of variation of metabolic parameters increased with the degree of polymerized MTP. The findings indicate that the organization of the cytoskeleton bestows coherence and robustness to the coordination of cellular metabolism.

Keywords: Glycolysis; Ethanolic fermentation; Pentose phosphate pathway; Microtubular protein; Mathematical modeling; Bifurcation and metabolic control analysis

Abbreviations: ATPase, adenosinetriphosphatase; G, glucose; G6P, glucose-6-phosphate; FDP, fructose-1,6 bisphosphate; G3P, glyceraldehyde-3-phosphate; DPG, 1,3-diphosphoglycerate; PEP, phosphoenolpyruvate; Py, pyruvate; IN, glucose uptake; HK, hexokinase; PFK, phosphofructokinase; G6PDH, glucose-6-phosphate dehydrogenase; ALD, aldolase; GAPD, glyceraldehyde-3-phosphate dehydrogenase; PGK, phosphoglycerate kinase; PK, pyruvate kinase; PKt, tetrameric form of PK; PKp, pentameric form of PK; TCA, tricarboxylic acid; ADH, branch to pyruvate decarboxylase-alcohol dehydrogenase; MTP, microtubular protein; C_D, dimeric microtubular protein bound to GDP; C_T, dimeric microtubular protein bound to GTP; C_P, microtubular protein integrating the microtubular structure

*Corresponding author. Johns Hopkins University, Institute of Molecular Cardiobiology, 720 Rutland Ave./Ross 844, Baltimore MD 21205, USA. Tel.: +1-410-955-2759; fax: +1-410-955-7953.

E-mail address: maon@bme.jhu.edu (M.A. Aon).

0301-4622/02/$ - see front matter
PII: S0301-4622(02)00056-X

1. Introduction

The spatio-temporal coordination of cellular function is a central problem in biology, and lies at the heart of understanding cell growth, proliferation, differentiation and functional adaptation toward environmental stimuli. Such coordination has been recognized in a number of biochemical processes, including signal transduction, gene expression, energetics and intermediary metabolism [1–3].

Two main ideas concerning the organization of metabolism in cells have emerged in the last few decades: (i) the concept of metabolic channeling, in which reactions are facilitated by product/substrate transfer between closely associated enzymes (stable or transient enzymatic complexes) (see [4], for a review); and (ii) cytoskeleton-driven modulation of enzymatic fluxes (see [1,2] for reviews). These two views are not mutually exclusive; however, a number of points have been made regarding the compatibility between models. It has been emphasized that metabolic channeling would not be favored on the surface of supramolecular structures [4] and a channeling complex cannot be predicted on the basis of binding data for several single enzymes. Two glycolytic enzymes, aldolase and PFK, individually bind to different domains of microtubules, but the formation of a complex between aldolase and PFK would preclude their binding to microtubules [5].

It has been shown that substantial increases in flux through chains of 1–3 enzymatic components may be achieved in the presence of microtubular protein [1,6,7]. However, the enhancement of flux depends on several factors, as follows: (i) the concentration of microtubular protein; (ii) the presence, for some enzymatic reactions, of microtubule associated proteins (MAPs) apart from tubulin, and (iii) the polymerization state of cytoskeletal proteins. Moreover, the type of cytoskeletal protein is also relevant, since there is evidence that certain enzymatic reactions are inhibited when incubated in the presence of F-actin, contrary to the actions of polymerized MTP [1,2,7].

Cytoskeletal dynamics play a crucial role in sensing and responding to osmotic stress [2,8,9]. In this regard, the cellular metabolic response to hormones such as insulin and glucagon depends on cell volume: swollen cells synthesize protein and glycogen, whereas shrunken cells catabolize these substances [8,9,15]. Cues associated with the spatial organization and orientation of cytoplasmic macromolecular assemblies are likely to regulate differential gene expression [10,11], signal transduction pathways [12,13], metastatic potential [14], and metabolic fluxes [2,6–8,15–19].

Microtubules, actin microfilaments and intermediate filaments represent an enormous protein surface in the cell. When calculated from the known size, shape, and concentration of the naked cytoskeleton, an estimate of 3000 μm^2 of surface area is obtained for a typical mammalian cell in culture [20]. The cytoskeleton provides an interface for binding a variety of proteins and enzymes. The binding affinity depends on several factors, including phosphorylation status [21–23], the presence of other proteins (e.g. MAPS, [1,6]), or the enzymatic activity of the protein [5,6]. Furthermore, protein binding also affects MT dynamics (see [1,2,13,19] for reviews).

Although a large amount of work has been done on the interactions between glycolytic enzymes and cytoskeletal proteins ([24,25], see [1] for a review), much less is known about the consequences of these interactions on the integrated fluxes through enzyme-catalyzed steps, or on signal amplification and transduction pathways [19]. Thus, the present work seeks to determine how the organization and dynamics of the tubulin cytoskeleton influences the biochemistry of living cells. More specifically, through mathematical modeling based on experimental evidence obtained in yeast, we address the question of whether the degree of microtubule polymerization affects the metabolic network through the glycolytic pathway, and/or its branches toward the pentose phosphate cycle, the TCA cycle and ethanol fermentation. The main finding shows that coherence and robustness are the two main features bestowed by the cytoskeleton to the modulation of the metabolic network. In this context, coherence means the integration of diverse elements and activities to produce a consistent response, whereas robustness refers to enhanced stability in the steady state dynamic

behavior of the metabolic network during variations in parametric conditions.

2. The mathematical model

2.1. Modeling microtubular protein dynamics and enzyme kinetics

2.1.1. Experimental background

In vitro studies. Experimental work done in vitro [1,2,6,7] showed that the presence of either polymerized or non-polymerized microtubular protein (MTP = tubulin + microtubule associated proteins, or MAPs) differentially modulate metabolic fluxes through the enzyme couples hexokinase/glucose 6-phosphate dehydrogenase (HK/G6PDH) and pyruvate kinase/lactate dehydrogenase (PK/LDH). The fluxes sustained through HK/G6PDH or PK/LDH enzymatic couples may be easily followed by NADPH production or NADH oxidation, respectively.

To assess the effect of polymerized or non-polymerized MTP, both enzymatic couples were assayed with different concentrations of MTP in the presence or in the absence of 2 mM GTP, respectively [6]. Under the assay conditions in vitro, the kinase in the enzymatic couple HK/G6PDH was in excess with respect to G6PDH, and thus the flux was proportional to the activity of the latter enzyme. In the PK/LDH system, the dehydrogenase was in excess; the flux then reflected the PK activity [6,7].

The effects of MTP concentration (polymerized or non-polymerized) on G6PDH or PK kinetics were assessed in two different ways: (i) by changes in the global flux sustained by the enzymatic couple through continuous monitoring of NADPH production or NADH oxidation, and (ii) by analyzing the initial velocity of the enzyme as a function of the enzyme's substrate (NADP or PEP) at fixed concentrations of polymerized or non-polymerized MTP in the stimulatory range.

The interaction of the enzymes with the microtubular lattice was investigated as follows [6,7]: (i) MTP was polymerized (37 °C for 30 min, monitored at 340 nm) in the presence or absence of the enzymatic couples, subsequently ultracentrifuged at $40\,000 \times g$ for 2 h, and the pellet and supernatant analyzed for enzymatic activity; and (ii) tubulin and MAPs were separated through a phosphocellulose column and tested for their effects on the enzymatic couples both separately or with reconstitution [6].

These experimental approaches allowed us to establish the following facts: (i) HK/G6PDH flux depended on the soluble, rather than polymerized, components of MTP; and (ii) the flux activation observed through the PK/LDH couple was mediated by the thermolabile MAPs component of the microtubular lattice [1,6,7]; and (iii) the presence of polymerized MTP induced an increase in cooperativity and the V_{max} of PK [6,7]. Based on these findings, we proposed and tested by mathematical modeling that PK may exist in two different oligomerization forms, i.e. tetramer and pentamer, with higher activity for the pentamer [7,17]. It was experimentally shown that MAPs might displace the equilibrium of PK oligomers from tetramers to pentamers [2,17]. The interaction of G6PDH and PK with MTP was suggested to be mediated by electrostatic interactions [6,26]. A similar scheme was proposed for the interaction of MAPs and PK [1,6].

In situ studies. We further investigated whether our results obtained in vitro had a cellular correlate by permeabilizing yeast cells and studying the sensitivity of G6PDH and PK kinetics to microtubule disassembly. The yeast *Saccharomyces cerevisiae* is a single-celled eukaryote that contains tubulin and actin in its cytoskeleton and can be easily permeabilized, providing an experimental tool for the intracellular assay of enzymes [6,27,28]. Nocodazole, which interferes with microtubule assembly, was used to determine if enzyme kinetics were influenced by microtubule assembly. The expected disassembly of microtubules induced by nocodazole was confirmed by direct immunofluorescence visualization of tubulin-containing structures [6]. The substrate dependence of PK or G6PDH rates was influenced in a manner similar to the in vitro results by microtubule polymerization (in the presence of taxol) or depolymerization (in the presence of nocodazole). Some quantitative differences in the kinetic parameters of both enzymes were noted in situ with respect to the in vitro data [2,6].

Thus, according to the experimental data obtained in vitro and in situ, we concluded that the dynamics of cytoskeleton and enzymatic reactions are regulated by the concentration of cytoskeletal protein; the local concentration of substrates, enzymes, or effectors; and the polymeric status of cytoskeletal components [1,2,19].

In vivo studies. The control analysis of glycolysis and the branches towards the TCA cycle and ethanol production, was previously elucidated in chemostat cultures of the yeast *S. cerevisiae* [29,30]. The matrix method of Metabolic Control Analysis was applied according to the rate expressions of each of the enzymes in the model, the levels of ATP, ADP, AMP, NAD, G6P + F6P, FdP, DHAP + G3P, 2PG, PEP, Pyr, and the main metabolic fluxes (O_2 and glucose consumption, CO_2 and ethanol production) determined in three different steady states for the wild-type yeast and three isogenic mutants for catabolite repression [30,31]. These studies were performed in chemostat cultures under aerobic conditions in the presence of glucose [30–32].

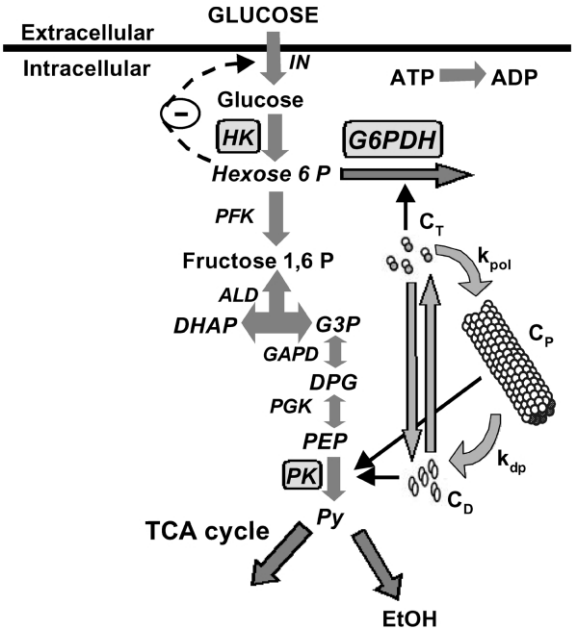

Fig. 1. A scheme of the metabolic network, the cycle of assembly–disassembly of MTP, and their interactions upon which the mathematical model is based. The cycle of assembly–disassembly of MTP is missing in the model in the absence of MTP.

2.2. Theoretical background

2.2.1. Glycolysis and the branches toward ethanol fermentation, the TCA cycle and the pentose phosphate pathways

The mathematical model of glycolysis utilized in the present work essentially consists of the steps depicted in Fig. 1. Briefly, the first two steps of the pathway are the sugar transport and HK (Fig. 1). Since the sugar transport step takes into account its inhibition by G6P, the inhibitory constant of G6P and the transmembrane glucose gradient are important parameters in the model (Fig. 1; Tables 1 and 2) [30]. The branch from G6P to the pentose phosphate (PP) pathway, catalyzed by G6PDH, is also considered. Since the enzymes phosphoglucose isomerase (PGI), phosphoglycero mutase (PGM) and enolase operate near equilibrium under intracellular conditions, they were not included in the model. Thus, the reactions catalyzed by these enzymes were lumped with the next reaction steps in the pathway, i.e. PGI with PFK and PGM and enolase with PK. In the case of PGI, the experimentally determined F6P concentration was added to G6P [30]. The branch leading to ethanol formation corresponds to lumped steps between the pyruvate decarboxylase-alcohol dehydrogenase, while the branch leading to the TCA cycle represents the pyruvate dehydrogenase-TCA cycle and oxidative phosphorylation [29].

ATP-consuming reactions related to pathways other than glycolysis were lumped in a general ATP-sink reaction. ATP was the only nucleotide considered as a state variable whereas NAD, NADH and AMP concentrations are parameters in our model [29].

2.2.2. The interaction and regulation of glycolytic enzymes and G6PDH by MTP

The equations that describe the MTP polymerization–depolymerization assume that tubulin may exist in three forms, polymerized (C_P); non-polymerized, bound to GTP (C_T); or non-polymerized, bound to GDP (C_D) (Fig. 1) [1,6,17,33,34]. A conservation equation relates the three forms of

Table 1
Model equations

Model equations: rate expressions

$$V^{\mathrm{IN}} = V^{\mathrm{IN}}_{\max}\frac{G_{\mathrm{o}}}{(K^{G}_{in}+G_{\mathrm{o}})\left(1+\dfrac{\mathrm{G6P}}{K^{e}_{in}}\right)} - \frac{G}{(K^{G}_{in}+G)\left(1+\dfrac{\mathrm{G6P}}{K^{e}_{in}}\right)} \tag{1}$$

$$V^{\mathrm{HK}} = V^{\mathrm{HK}}_{\max}\frac{1}{\left(1+\dfrac{K^{\mathrm{G}}_{s}K^{\mathrm{ATP}}_{m}}{\mathrm{G\ ATP}}+\dfrac{K^{\mathrm{G}}_{m}}{\mathrm{G}}+\dfrac{K^{\mathrm{ATP}}_{m}}{\mathrm{ATP}}\right)} \tag{2}$$

$$V^{\mathrm{PFK}} = V^{\mathrm{PFK}}_{\max}\frac{g_r\dfrac{\mathrm{G6P}}{K^{\mathrm{G6P}}_{r}}\dfrac{\mathrm{ATP}}{K^{\mathrm{ATP}}_{r}}\left(1+\dfrac{\mathrm{G6P}}{K^{\mathrm{G6P}}_{r}}+\dfrac{\mathrm{ATP}}{K^{\mathrm{ATP}}_{r}}+g_r\dfrac{\mathrm{G6P}}{K^{\mathrm{G6P}}_{r}}\dfrac{\mathrm{ATP}}{K^{\mathrm{ATP}}_{r}}\right)^{(n1-1)}}{\left(1+\dfrac{\mathrm{G6P}}{K^{\mathrm{G6P}}_{r}}+\dfrac{\mathrm{ATP}}{K^{\mathrm{ATP}}_{r}}+g_r\dfrac{\mathrm{G6P}}{K^{\mathrm{G6P}}_{r}}\dfrac{\mathrm{ATP}}{K^{\mathrm{ATP}}_{r}}\right)^{n1}+L_0\left(\dfrac{1+\dfrac{c_{\mathrm{AMP}}\,\mathrm{AMP}}{K^{\mathrm{AMP}}_{r}}}{1+\dfrac{\mathrm{AMP}}{K^{\mathrm{AMP}}_{r}}}\right)^{n1}\left(1+\dfrac{c_{\mathrm{G6P}}\,\mathrm{G6P}}{K^{\mathrm{G6P}}_{r}}+\dfrac{c_{\mathrm{ATP}}\,\mathrm{ATP}}{K^{\mathrm{ATP}}_{r}}+g_t\dfrac{c_{\mathrm{G6P}}\,\mathrm{G6P}}{K^{\mathrm{G6P}}_{r}}\dfrac{c_{\mathrm{ATP}}\,\mathrm{ATP}}{K^{\mathrm{ATP}}_{r}}\right)^{n1}} \tag{3}$$

$$V^{\mathrm{G6PDH}} = \frac{\mathrm{V}^{\mathrm{G6PDH}}_{\max}}{\left(\dfrac{K_{\mathrm{G6P}}K_{\mathrm{NADP}}}{\mathrm{G6P\ NADP}}+\dfrac{K_{\mathrm{G6P}}}{\mathrm{G6P}}+\dfrac{K_{\mathrm{NADP}}}{\mathrm{NADP}}+1\right)}+\frac{\mathrm{V}^{\mathrm{G6PDH(II)}}_{\max}}{\left(\dfrac{K_{\mathrm{G6P}}K'_{\mathrm{NADP}}K_{\mathrm{TUB}}}{\mathrm{G6P\ NADP\ TUB}}+\dfrac{K_{\mathrm{G6P}}K'_{\mathrm{NADP}}}{\mathrm{G6P\ NADP}}+\dfrac{K'_{\mathrm{NADP}}K_{\mathrm{TUB}}}{\mathrm{NADP\ TUB}}+\dfrac{K_{\mathrm{G6P}}K_{\mathrm{TUB}}}{\mathrm{G6P\ TUB}}+\dfrac{K_{\mathrm{TUB}}}{\mathrm{TUB}}+\dfrac{K_{\mathrm{G6P}}}{\mathrm{G6P}}+\dfrac{K'_{\mathrm{NADP}}}{\mathrm{NADP}}+1\right)} \tag{4}$$

where $\mathrm{TUB} = \mathrm{C_T} + \mathrm{C_D}$

$$V^{\mathrm{ALD}} = \frac{V^{\mathrm{ALD}}_{\max}\dfrac{\mathrm{FDP}}{K^{\mathrm{FDP}}_{m}} - V^{\mathrm{ALD}(r)}_{\max}\dfrac{\mathrm{G3P}}{K^{\mathrm{G3P}}_{m}}}{\left(1+\dfrac{\mathrm{FDP}}{K^{\mathrm{FDP}}_{m}}+\dfrac{\mathrm{G3P}}{K^{\mathrm{G3P}}_{in}}\right)} \tag{5}$$

$$V^{\mathrm{GAPDH}} = \frac{V^{\mathrm{GAPDH}}_{\max}}{\left(1+\dfrac{K_{\mathrm{G3P}}}{\mathrm{G3P}}+\dfrac{K_{\mathrm{NAD}}}{\mathrm{NAD}}\left(1+\dfrac{\mathrm{AMP}}{K_1}+\dfrac{\mathrm{ADP}}{K_2}+\dfrac{\mathrm{ATP}}{K_3}\right)+\dfrac{K_{\mathrm{G3P}}K_{\mathrm{NAD}}}{\mathrm{G3P\ NAD}}\left(1+\dfrac{\mathrm{NADH}}{K^{\mathrm{NADH}}_{i}}\right)\left(1+\dfrac{\mathrm{AMP}}{K_1}+\dfrac{\mathrm{ADP}}{K_2}+\dfrac{\mathrm{ATP}}{K_3}\right)\right)} \tag{6}$$

$$V^{\mathrm{PGK}} = \frac{V^{\mathrm{PGK}}_{\max}\mathrm{DPG}}{(K^{\mathrm{DPG}}_{m}+\mathrm{DPG})} \tag{7}$$

Table 1 *(Continued)*

Model equations: rate expressions

$$V^{\mathrm{PK}}=\frac{V_{\max}^{\mathrm{PK}}}{1+\dfrac{K_{\mathrm{pH}}}{\mathrm{H}^{+}}}\frac{\dfrac{g_r^{\mathrm{PK}}\dfrac{\mathrm{PEP}}{K_r^{\mathrm{PEP}}}\dfrac{\mathrm{ADP}}{K_r^{\mathrm{ADP}}}R^{n-1}+L_{\mathrm{o}}^{\mathrm{PK}}\left(\dfrac{1+\dfrac{c_{\mathrm{FDP}}\mathrm{FDP}}{K_r^{\mathrm{FDP}}}}{1+\dfrac{\mathrm{FDP}}{K_r^{\mathrm{FDP}}}}\right)^{n}\dfrac{\mathrm{FDP}}{K_r^{\mathrm{FDP}}}g_t^{\mathrm{PK}}\dfrac{c_{\mathrm{PEP}}\mathrm{PEP}}{K_r^{\mathrm{PEP}}}\dfrac{c_{\mathrm{ADP}}\mathrm{ADP}}{K_r^{\mathrm{ADP}}}T^{n-1}}{R^{n}+L_{\mathrm{o}}^{\mathrm{PK}}\left(\dfrac{1+\dfrac{c_{\mathrm{FDP}}\mathrm{FDP}}{K_r^{\mathrm{FDP}}}}{1+\dfrac{\mathrm{FDP}}{K_r^{\mathrm{FDP}}}}\right)^{n}T^{n}} \tag{8}$$

being

$$R=1+\frac{\mathrm{PEP}}{K_r^{\mathrm{PEP}}}+\frac{\mathrm{ADP}}{K_r^{\mathrm{ADP}}}+g_r^{\mathrm{PK}}+\frac{\mathrm{PEP}}{K_r^{\mathrm{PEP}}}\frac{\mathrm{ADP}}{K_r^{\mathrm{ADP}}}$$

$$T=1+\frac{c_{\mathrm{PEP}}\mathrm{PEP}}{K_r^{\mathrm{PEP}}}+\frac{c_{\mathrm{ADP}}\mathrm{ADP}}{K_r^{\mathrm{ADP}}}+g_t^{\mathrm{PK}}+\frac{c_{\mathrm{PEP}}\mathrm{PEP}}{K_r^{\mathrm{PEP}}}\frac{c_{\mathrm{ADP}}\mathrm{ADP}}{K_r^{\mathrm{ADP}}}$$

with $V_{\max}^{\mathrm{PK}}=V_{\max}^{\mathrm{PK}t}+(V_{\max}^{\mathrm{PK}p}-V_{\max}^{\mathrm{PK}t})\dfrac{\mathrm{PK_P}}{\mathrm{C_{PK}}}$

and $n=4+\dfrac{\mathrm{PK_P}}{\mathrm{C_{PK}}}$

$$V^{\mathrm{TCA}}=\frac{V_{\max}^{\mathrm{TCA}}\mathrm{Py}^2}{(K_m^{\mathrm{Py}})^2+\mathrm{Py}^2} \tag{9}$$

$$V^{\mathrm{ADH}}=\frac{V_{\max}^{\mathrm{ADH}}\mathrm{Py}}{K'^{\mathrm{Py}}_m+\mathrm{Py}} \tag{10}$$

$$V^{\mathrm{ATPase}}=K^{\mathrm{ATP}}\mathrm{ATP} \tag{11}$$

Conservation relations:

$$C_{\mathrm{n}}=\mathrm{ATP}+\mathrm{ADP}+\mathrm{AMP} \tag{12}$$

$$C_{\mathrm{MTP}}=\mathrm{C_D}+\mathrm{C_T}+\mathrm{C_P} \tag{13}$$

$$C_{PK}=\mathrm{PK_T}+\mathrm{PK_P} \tag{14}$$

Ordinary differential equations*:

$$\frac{\mathrm{d}G}{\mathrm{d}t}=V^{\mathrm{IN}}-V^{\mathrm{HK}} \tag{15}$$

Table 1 *(Continued)*

Model equations: rate expressions	
$\frac{\mathrm{dG6P}}{\mathrm{d}t} = V^{\mathrm{HK}} - V^{\mathrm{PFK}} - V^{\mathrm{G6PDH}}$	(16)
$\frac{\mathrm{dFDP}}{\mathrm{d}t} = V^{\mathrm{PFK}} - V^{\mathrm{ALD}}$	(17)
$\frac{\mathrm{dG3P}}{\mathrm{d}t} = 2V^{\mathrm{ALD}} - V^{\mathrm{GAPDH}}$	(18)
$\frac{\mathrm{dDPG}}{\mathrm{d}t} = V^{\mathrm{GAPDH}} - V^{\mathrm{PGK}}$	(19)
$\frac{\mathrm{dPEP}}{\mathrm{d}t} = V^{\mathrm{PGK}} - V^{\mathrm{PK}}$	(20)
$\frac{\mathrm{dPy}}{\mathrm{d}t} = V^{\mathrm{PK}} - V^{\mathrm{TCA}} - V^{\mathrm{ADH}}$	(21)
$\frac{\mathrm{dATP}}{\mathrm{d}t} = -V^{\mathrm{HK}} - V^{\mathrm{PFK}} + V^{\mathrm{PGK}} + V^{\mathrm{PK}} + \mathrm{PO}\, V^{\mathrm{TCA}} - V^{\mathrm{ATP}}$	(22)
$\frac{\mathrm{dPK_P}}{\mathrm{d}t} = 0.1k_{\mathrm{p2}}\mathrm{PK_T}\mathrm{C_P} - k_{\mathrm{p3}}\mathrm{PK_P} - k_4\mathrm{PK_P}\mathrm{GTP}$	(23)
$\frac{\mathrm{dC_T}}{\mathrm{d}t} = -k_{\mathrm{pol}}\mathrm{C_T}(\mathrm{C_P})^2 - k_{\mathrm{f}}\mathrm{C_D} - k_{\mathrm{b}}\mathrm{C_T}\mathrm{GDP}$	(24)
$\frac{\mathrm{dC_P}}{\mathrm{d}t} = k_{\mathrm{pol}}\mathrm{C_T}(\mathrm{C_P})^2 - k_{\mathrm{dp}}\mathrm{C_P}$	(25)

* In the model in the absence of MTP, Eqs. (23–25) do not take part of the system. All PK is considered to be in its tetrameric state, thus the corresponding $V_{\mathrm{max}}^{\mathrm{PK}}$ and n take the values of the tetrameric form of the enzyme (see also Eq. (8) and Table 2).

Table 2
Parameters and variables of the model studied.

Name	Description (units)	Eq.	Value	Ref.[a]
V_{max}^{IN}	Maximal rate of glucose uptake (IN) (mM min^{-1})	1	10.0	1, 2
K_{in}^{G}	Michaelis–Menten constant of glucose transport (mM)	1	0.001	1, 2
K_{in}^{e}	Inhibition constant of transport by G6P (mM)	1	12.0	1, 2
G_o	Extracellular glucose concentration (mM)	1	1.0	1, 2
V_{max}^{HK}	Maximal rate of hexokinase (HK) (mM min^{-1})	2	13.0	1, 3, 4
K_m^{ATP}	Michaelis–Menten constant of HK for ATP (mM)	2	0.1	1, 3, 4
K_s^{G}	Michaelis–Menten constant of HK for glucose (mM)	2	0.0062	1, 3, 4
K_m^{G}	Michaelis–Menten constant of HK for glucose (mM)	2	0.11	1, 3, 4
V_{max}^{PFK}	Maximal rate of phosphofructokinase (PFK) (mM min^{-1})	3	30.0	1, 3, 4
K_r^{G6P}	Microscopic dissociation constant of G6P in the R state (mM)[b]	3	1.0	1, 3, 4, 8, 9
K_r^{ATP}	Microscopic dissociation constant of ATP in the R state (mM)	3	0.06	1, 3, 4, 8, 9
K_r^{AMP}	Microscopic dissociation constant of AMP in the R state (mM)	3	0.025	1, 3, 4, 8, 9
L_o	Equilibrium constant for the R↔T transition	3	25 000	1, 3, 4, 8, 9
c_{G6P}	Ratio of the microscopic dissociation constants K_R/K_T with respect to G6P[b]	3	0.0005	1, 3, 4, 8, 9
c_{ATP}	Ratio of the microscopic dissociation constants K_R/K_T with respect to ATP	3	1.0	1, 3, 4, 8, 9
c_{AMP}	Ratio of the microscopic dissociation constants K_R/K_T with respect to AMP	3	0.019	1, 3, 4, 8, 9
$n1$	Number of PFK subunits (protomers) and homologous ligand binding sites	3	2	1, 3, 4, 8, 9
G_r	Affinity coefficient for the substrates at the R state	3	10	1, 3, 4, 8, 9
V_{max}^{G6PDH}	Maximal rate of G6PDH from the MTP independent term (mM min^{-1})	4	1.6	5, 6
$V_{max}^{G6PDH(II)}$	Maximal rate of G6PDH from the MTP-dependent term (mM min^{-1})	4[c]	1.0	5, 6
K_{G6P}	Kinetic constant of G6PDH on G6P (mM)	4	0.05	5, 6
K_{NADP}	Kinetic constant of G6PDH on NADP (mM)	4	0.05	5, 6
K_{TUB}	Kinetic constant of G6PDH on soluble MTP (TUB) (mM)	4	0.4	5, 6
K'_{NADP}	Kinetic constant of G6PDH on NADP (mM)	4	0.05	5, 6
TUB	Refers to the sum of the non-polymeric (soluble) forms of microtubular protein = $C_D + C_T$ (mM)	4		5, 6
NADP	Concentration of the oxidized form of NADP (mM)	4	1.0	5, 6
V_{max}^{ALD}	Maximal rate of aldolase (ALD) in the sense of G3P (mM min^{-1})	5	2.5	1, 3, 4
$V_{max}^{ALD(r)}$	Maximal rate of ALD in the sense of FDP (mM min^{-1})	5	1.0	1, 3, 4
K_m^{G3P}	Michaelis–Menten constant of ALD for G3P (mM)	5	20.0	1, 3, 4
K_m^{FDP}	Michaelis–Menten constant of ALD for FDP (mM)	5	0.5	1, 3, 4
V_{max}^{GAPDH}	Maximal rate of Glyceraldehyde 3-P dehydrogenase (GAPDH) (mM min^{-1})	6	10.0	1, 3, 4
K_{G3P}	Kinetic constant of GAPDH for G3P (mM)	6	0.0025	1, 3, 4
K_{NAD}	Kinetic constant of GAPDH for NAD (mM)	6	0.18	1, 3, 4
K_i^{NADH}	Inhibition constant of G6PDH for NADH (mM)	6	0.0003	1, 3, 4
NAD	NAD concentration (mM)	6	1.0	1, 3, 4
NADH	NADH concentration (mM)	6	0.01	1, 3, 4
K_1	Kinetic constant of GAPDH for AMP (mM)	6	1.1	1, 3, 4
K_2	Kinetic constant of GAPDH for ADP (mM)	6	1.5	1, 3, 4
K_3	Kinetic constant of GAPDH for ATP (mM)	6	2.5	1, 3, 4
V_{max}^{PGK}	Maximal rate of PGK (mM min^{-1})	7	3.0	1, 3, 4
K_m^{DPG}	Michaelis Menten constant of PGK for DPG (mM)	7	0.002	1, 3, 4

Table 2 *(Continued)*

Name	Description (units)	Eq.	Value	Ref.[a]
$V_{\max}^{PKt}$	Maximal rate of PK tetrameric form (mM min^{-1})	8	25.0	5, 6, 7
$V_{\max}^{PKp}$	Maximal rate of PK pentameric form (mM min^{-1})	8	50.0	5, 6, 7
K_{pH}	Equilibrium constant for acid dissociation of PK	8	9.5×10^{-9}	1, 3, 4
H^+	Proton concentration (mM)	8	3.2×10^{-8}	1, 3, 4
g_r^{PK}	Affinity coefficient for the substrates at the R state	8	0.1	1, 3, 4, 8, 9
g_t^{PK}	Affinity coefficient for the substrates at the T state	8	1.0	1, 3, 4, 8, 9
K_r^{PEP}	Microscopic dissociation constant of PEP in the R state (mM)	8	1.0	1, 3, 4, 8, 9
K_r^{ADP}	Microscopic dissociation constant of ADP in the R state (mM)	8	0.06	1, 3, 4, 8, 9
K_r^{FDP}	Microscopic dissociation constant of FDP in the R state (mM)	8	0.025	1, 3, 4, 8, 9
L_o^{PK}	Equilibrium constant for the R↔T transition	8	1,000	1, 3, 4, 8, 9
c_{PEP}	Ratio of the microscopic dissociation constants K_R/K_T with respect to PEP	8	0.02	1, 3, 4, 8, 9
c_{ADP}	Ratio of the microscopic dissociation constants K_R/K_T with respect to ADP	8	1.0	1, 3, 4, 8, 9
c_{FDP}	Ratio of the microscopic dissociation constants K_R/K_T with respect to FDP	8	0.01	1, 3, 4, 8, 9
n	Number of PK subunits (protomers) and homologous ligand binding sites	3	4	1, 3, 4, 8, 9
$V_{\max}^{TCA}$	Maximal rate of the TCA cycle (mM min^{-1})	9	10.0	1, 3, 4
K_m^{Py}	Kinetic constant of the TCA cycle for Py (mM)	9	0.329	1, 3, 4
$V_{\max}^{ADH}$	Maximal rate of the pyruvate decarboxylase–alkohol dehydrogenase catalyzed branch (ADH) (mM min^{-1})	10	0.5	1, 3, 4
K'^{Py}_m	Kinetic constant of ADH for Py (mM)	10	0.169	1, 3, 4
K_{ATP}	Kinetic rate constant of ATPase (min^{-1})	11	5.0	1, 3, 4
C_n	Total concentration of adenine nucleotides (mM)	12	9.0	1, 3, 4
AMP	AMP concentration (mM)	12	0.5	1, 3, 4
C_{MTP}	Total concentration of microtubular protein (mM)	13	0.9	5, 6, 7
C_{PK}	Total concentration of PK (mM)	14	0.01	5, 6, 7
PO	Stoichiometry of ATP production in TCA cycle and respiration	22	4.0	1, 3, 4
k_{p2}	Rate constant of PKt and PKp interconversion(mM^{-1} min^{-1})	23	10.0	5, 6, 7
k_{p3}	Rate constant of PKt and PKp interconversion (min^{-1})	23	0.05	5, 6, 7
k_4	Rate constant of PKt and PKp interconversion(mM^{-1} min^{-1})	23	0.02	5, 6, 7
GTP	GTP concentration (mM)	23	0.95	5, 6, 7
GDP	GDP concentration (mM)	24	0.05	5, 6, 7
k_{pol}	Rate constant of MTP polymerization (mM^{-2} min^{-1})	24	10.0	5, 6, 7
k_f	Rate constant of GTP binding to TUB (min^{-1})	24	3.0	5, 6, 7
k_b	Rate constant of GTP hydrolysis by TUB (mM^{-1} min^{-1})	24	2.5	5, 6, 7
k_{dp}	Rate constant of MTP depolymerization (min^{-1})	25	0.0025	5, 6, 7

[a] 1. [30]; 2. [43]; 3. [29]; 4. [44]; 5. [6]; 6. [1]; 7. [7]; 8. [45]; 9. [46].

[b] G6P and F6P are considered to equilibrate rapidly assuming that phosphoglucoisomerase is fast enough.

[c] In the model without interaction with MTP, the term containing this parameter in Eq. 4 annihilates.

MTP [Eq. (13)]. The mathematical modeling of MTP assembly–disassembly [Eqs. (24,25)] was tested by simulation of polymerization kinetics under in vitro conditions [6,7].

2.2.3. Pyruvate kinase

The activation mechanism of PK by MTP was modeled taking into account that MTP promoted an increase in the degree of co-operativity exhibited by the enzyme. This change in co-operativity favored the idea that, in the presence of either polymerized- or non-polymerized-MTP, the average degree of self-association increased together with the maximal activity of the enzyme [6,7]. A partial model of the interaction between the microtubular lattice with PK, favoring the formation of enzymatic states of higher oligomerization, was previously developed [1,6,17]. In the presence of MTP, PK may exist as a tetramer (T) or pentamer (P). The proportion of P depends on the polymeric status of MTP, with a higher V_{max}^{PK} for P than T (see Eqs. (8) and (23) in Table 1) [1,6,17]. The coupling with the polymeric status of MTP is realized through the term of P formation that is proportional to the amount of polymerized MTP, C_P, with 0.1 as the proportionality constant that accounts for the fact that MAPs represent 10% of total MTP [Eq. (23)] [6].

2.2.4. Glucose 6 phosphate dehydrogenase

The modeling of G6PDH kinetics takes into account the effects exerted by MTP as described in Section 2.1.1 above. Briefly, the rate expression of G6PDH comprises MTP-dependent and -independent terms [Eq. (4)]. The soluble component of MTP (i.e. not participating in the microtubular lattice) could account for the activation of the flux through this enzyme that does not interact strongly or permanently with the assembled MTP [6]. This was assessed by the ability of the rate expression of G6PDH to fit the experimental data [6]. The maximal initial rates of G6PDH utilized in the model, were those obtained experimentally in the absence or the presence of MTP.

2.3. Model formulation

Fig. 1 shows a scheme of the metabolic network, the cycle of assembly–disassembly of MTP and their links. The metabolic network represents glycolysis and the branch toward the PP pathway, TCA cycle and ethanol production in the yeast *S. cerevisiae*. The model behavior was simulated through a set of 11 ordinary differential equations (ODEs 15–25 in Table 1) and conservation relations [Eqs. (12–14) in Table 1) whose parameter values are described in Table 2. Three of the state variables of the model concern the polymeric status of MTP, namely the equations describing the evolution of polymerized, C_P, and non-polymerized, C_T, MTP, and the dynamics of oligomerization of PK (between tetrameric and pentameric forms) [Eqs. (23–25)].

2.4. Parameter optimization and simulation conditions of the mathematical model

The individual rate laws described by Eqs. (1–11) were derived from the enzyme kinetics in vitro. The kinetic constants were taken from the literature as indicated in Cortassa and Aon [29,30]. However, we have optimized the V_{max} of each rate equation so as to reproduce experimental data obtained at steady states achieved by *S. cerevisiae* in our chemostat cultures [30,32]. Three criteria were chosen to perform a parameter optimization: (a) the system of ODEs should attain a steady state; (b) the flux through glycolysis should be equal to the experimentally measured flux of glucose consumption; and (c) the metabolite levels should match the experimentally determined steady state concentrations. In our hands, it was seen that V_{max} rather than K_m values were the most sensitive to the optimization procedure, suggesting that the former could be more affected by differences between in vitro and in vivo data.

2.5. Metabolic control analysis (MCA)

The matrix method of MCA [35,36] was applied to determine the rate-controlling steps of the flux and metabolite concentration control coefficients [29,30]. The metabolite concentrations at each steady state were introduced into the derivatives of the rate equations with respect to each metabolite concentration, in order to calculate the elasticity coefficients for constructing the

corresponding matrix **E**. The inversion of matrix **E** results in the matrix of control coefficients C, whose first column contains the flux control coefficients. The matrix **E** was inversed using standard mathematical software (e.g. Maple, Matlab, Mathematica).

2.6. Dynamic bifurcation analysis (DBA)

Dynamic bifurcation theory permits analysis of the qualitative dynamic behavior of any system of equations in terms of type and stability of the steady states exhibited when a parameter (called a bifurcation parameter) is varied [1,37–39]. This characterization produces a bifurcation diagram (see, e.g. Fig. 2). The parameter values for which the stability properties change (e.g. from stable to unstable steady states) are called bifurcation points. A visualization of the ensemble of steady states and the localization of the bifurcation points may be obtained with DBA. We applied DBA based on the numerical analysis of ordinary differential equations (ODEs) that was performed with AUTO, a software designed for continuation and bifurcation analysis of ODEs that can be applied to the study of non-linear systems [39]. The numerical procedure used by AUTO is based on an analysis of the Jacobian of the system with a Newton chord method and the following is computed: (i) branches of solutions of stable or unstable steady states, either asymptotic or periodic; (ii) evaluation of the eigenvalues and accordingly the stability of such branches; (iii) location of bifurcation points, limit points, Hopf bifurcation points and computation of the bifurcating branches [39].

2.7. A numerical approach for control analysis of metabolic networks

The description of a particular network of reactions or processes implies the characterization of all possible steady states that may be attained by this particular network [1]. DBA makes possible the analysis of the steady state of a system continuously as a function of a bifurcation parameter. Thus, as an alternative to the matrix method of MCA, the flux or concentration control coefficients can be obtained straightforwardly from the first derivative of bifurcation diagrams plotted in double logarithmic form. Otherwise stated, the slope of the log–log form of the bifurcation diagram allows a graphical and ready estimate of the control exerted on the flux or a metabolite concentration, by a parameter under study [1].

3. Results

In order to seek whether the degree of cytoskeleton polymerization could exert systemic effects on the glycolytic flux, we attempted to change the relative level of polymerized to non-polymerized MTP. The rate constants of MTP depolymerization, k_{dp}, or polymerization, k_{pol}, were varied in order to achieve different levels of polymerized MTP, C_P. With this rationale in mind we sought to unravel whether the extent of polymerization of MTP could affect the dynamics of the whole metabolic network.

3.1. Effects of the polymeric status of MTP on the glycolytic flux

3.1.1. Shifting the control of the flux partition between pathways

We performed stability and bifurcation analyses of the mathematical model as a function of parameters related with the dynamics of assembly–disassembly of MTP. The level of polymerized MTP, C_P, was changed through variation of the rate constant k_{dp}. Fig. 2 shows the flux ratio of glycolysis over the PP pathway, and some selected fluxes through individual enzymatic steps (Fig. 2b) and metabolite concentrations (Fig. 2a), at different levels of the metabolic network, as a function of the rate of microtubules depolymerization, k_{dp}.

The change in k_{dp} brings about changes in the rates and metabolites concentration throughout the network (Fig. 2a,b). Phase plane analysis shows that the flux through glycolysis increases with higher levels of C_P (Fig. 2c). Similar results were obtained when the behavior of the system was analyzed as a function of the rate constant of MTP polymerization, k_{pol} (Fig. 2c, inset). Concomitant to the global flux modulation, the steady state

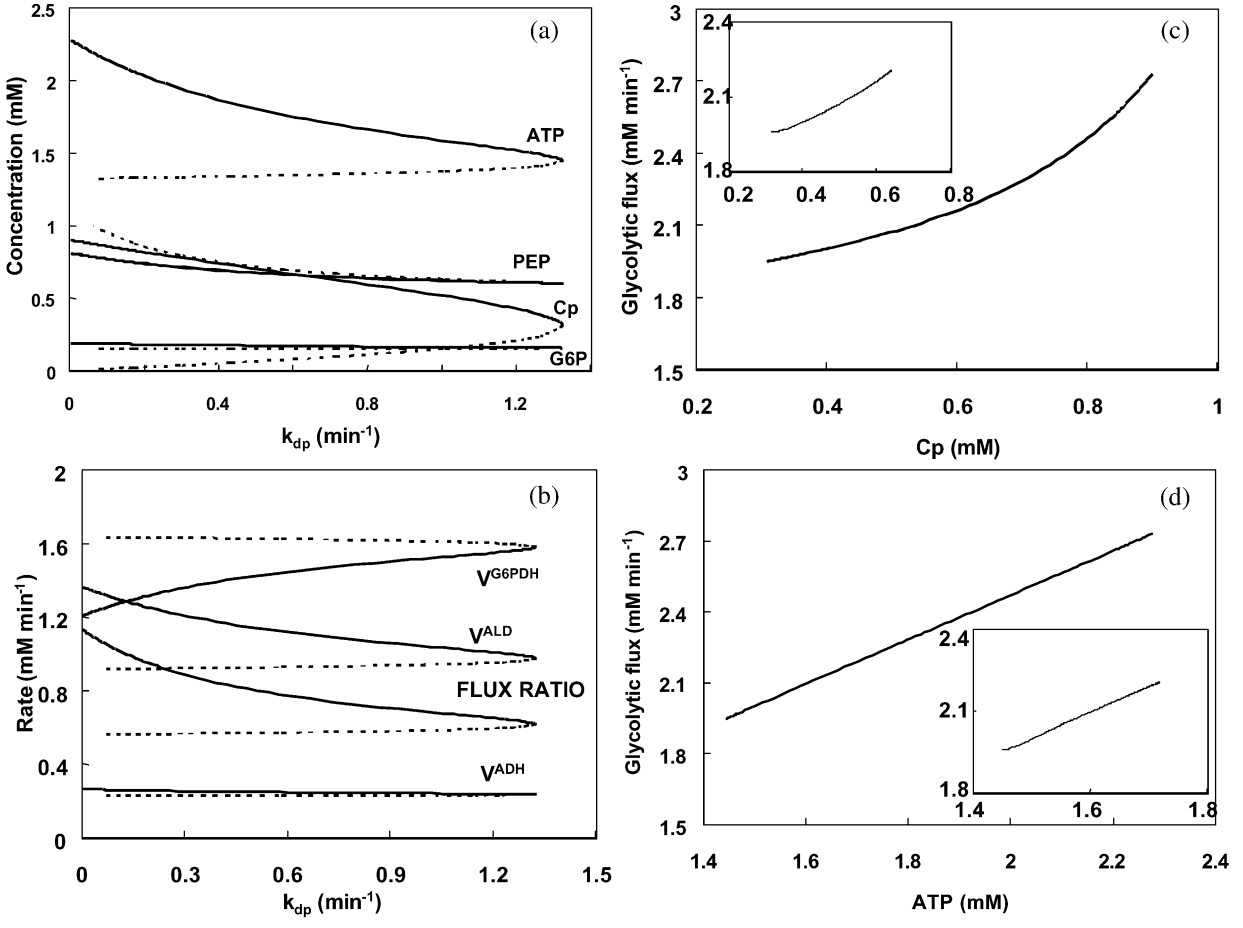

Fig. 2. Stability and bifurcation analyses of the mathematical model as a function of the depolymerization, k_{dp}, and polymerization, k_{pol}, constants of MTP. The steady state behavior and stability of the mathematical model, as well as the existence of bifurcation points, were analyzed as a function of parameters related with the assembly–disassembly of MTP. In c and d, the main panels show the results obtained through variation of k_{dp} whereas the insets correspond to the simulations performed with k_{pol}. Also shown is the steady state behavior of metabolite concentrations as state variables of the model (a) and the fluxes through individual enzymatic steps as functions of state variables (b). For the sake of clarity only some metabolites and fluxes are represented, placed at different levels of the metabolic network. Also depicted are the phase plane analyses of the glycolytic flux as a function of the level of polymerized MTP, C_P (c), or ATP concentration (d). The insets belong to the results obtained with model simulations as a function of k_{pol} and the axis correspond to the same variables and units as in main panels. The model parameters are shown in Table 2.

concentration of metabolites also changed systemically (Fig. 2a). Particularly, the glycolytic flux and ATP co-varied either when k_{dp} or k_{pol} were changed (Fig. 2d, see also inset). That the alterations induced by the polymeric status of MTP on the metabolic network were systemic was confirmed by varying individual kinetic parameters of enzymes coupled to MTP dynamics such as PK. In the latter case, only local changes in the level of metabolites (i.e. PEP) affected by the enzyme activity were observed (results not shown).

At high rates of microtubule depolymerization, the system bifurcates, as revealed by the existence of limit points giving rise to unstable branches of steady states either of metabolites or enzymatic rates (Fig. 2a,b, dashed lines).

Taken together, these results are in agreement with a coherent, coordinated, modulation of the glycolytic flux exerted by the tubulin cytoskeleton through its degree of polymerization. In order to unravel the mechanism of this effect, we applied MCA at high (99% of the total pool of MTP, C_{MTP}) or low (45% of the total pool of MTP, C_{MTP}) levels of polymerized MTP. The main question is whether the structure of control of the pathway changes depending on the degree of polymerization of the cytoskeleton. The results obtained are shown in Fig. 3. Glucose uptake, HK and the PP pathway branch are the main rate-controlling steps (the two former are positive and the latter negative) either at high or low levels of C_P. High levels of the polymer decrease the negative control exerted by the branch to the PP pathway over glycolysis, thus allowing higher fluxes through the network (Fig. 3a). The latter explains why the glycolytic flux increases with increasing degree of polymerization of the tubulin cytoskeleton (Fig. 2c). Thus, the polymeric status of MTP may exert its modulation of the metabolic flux through shifting the flux partition between pathways at branch points.

Panel (b) of Fig. 3 shows that the concentration of ATP is controlled by the main rate-controlling steps of the flux. In fact, the ATP concentration, as a 'systemic' variable, i.e. implied in several steps of the network, is controlled positively by the uptake, HK, PFK and the branch to the TCA cycle, and negatively by the branch to the PP

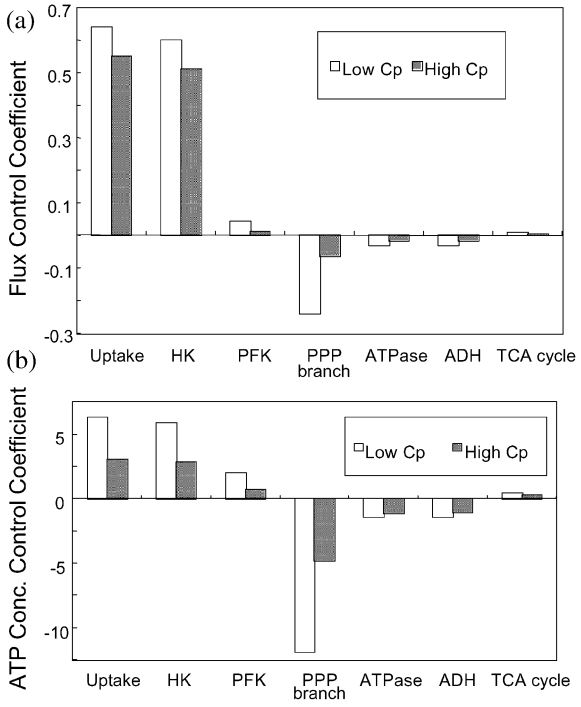

Fig. 3. Metabolic control analysis of the model. The matrix method of MCA was applied. Shown are the flux (a) and the ATP concentration (b) control coefficients of the steps indicated in abscissas, obtained with the set of parameters indicated in Table 2. The values of k_{pol} were 8.05 and 10.0 mM^{-2} min^{-1}, whereas $k_{dp} = 1.12$ and 0.022 min^{-1}, for low and high C_P levels, respectively.

pathway, the ATPase and the alcohol dehydrogenase-catalyzed step (Fig. 3b). A more even distribution of the control over the ATP concentration is observed at high amounts of the polymer.

3.1.2. Modulating the control of the PP branch and increasing the robustness of the metabolic network behavior

In order to further substantiate and clarify the modulatory role exerted by the polymeric status of the tubulin cytoskeleton over the flux control by the PP pathway on glycolysis, we compared the behavior of the mathematical model with or without MTP. More specifically, the G6PDH step that catalyzes the branch toward the PP pathway possesses two terms, one MTP-dependent characterized by $V_{max}^{G6PDH(II)}$, and the other MTP-independent,

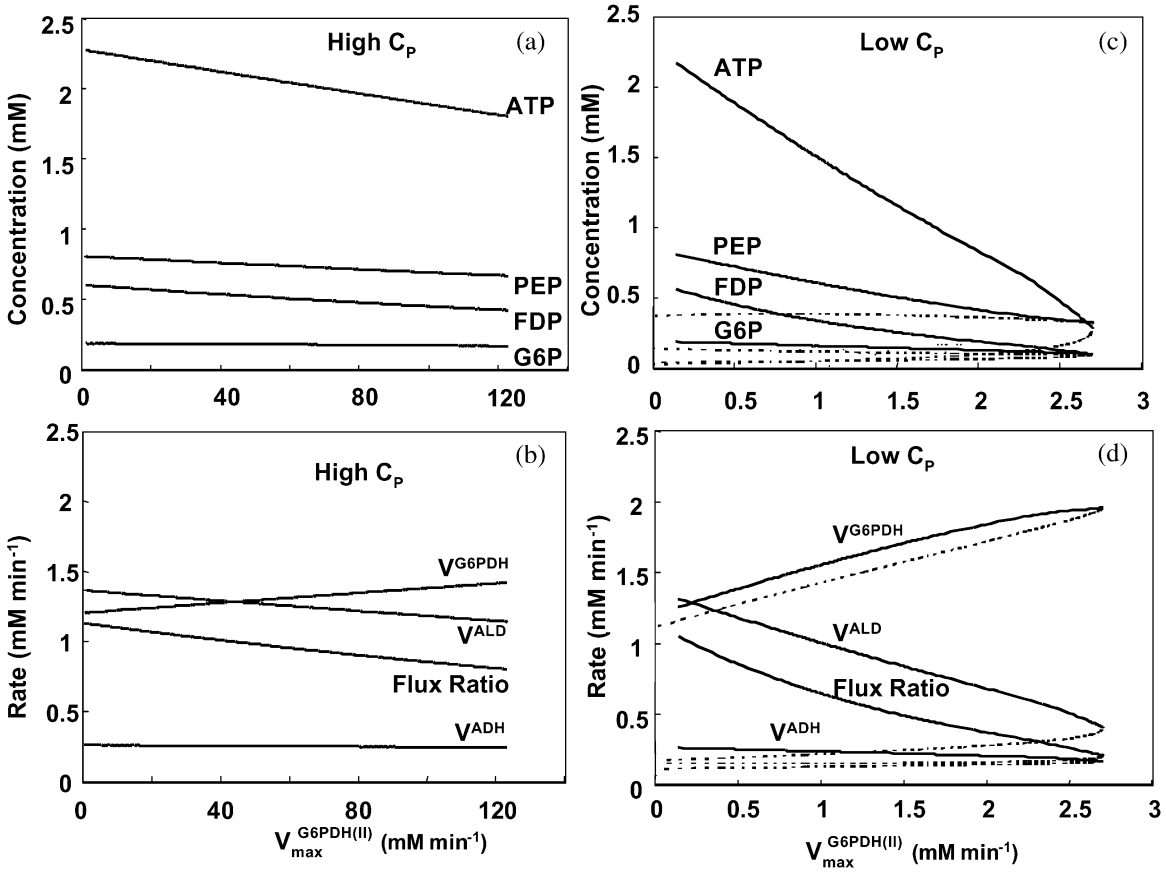

Fig. 4. Stability and bifurcation analyses of the mathematical model as a function of $V_{max}^{G6PDH(II)}$. The steady state behavior and stability of the mathematical model as well as the existence of bifurcation points were analyzed as a function of $V_{max}^{G6PDH(II)}$ in the presence of high (a,b: 99% of the total pool of MTP, C_{MTP}) or low (c,d: 45% of the total pool of MTP, C_{MTP}) C_P. For clarity, the top panels (a,c) only show the concentration of selected metabolites that represent different portions of the metabolic pathway. In the lower panels (b,d), the flux ratio of aldolase over the PP pathway, V^{ALD}/V^{G6PDH}, and some fluxes through individual enzymatic steps are depicted. The model in the absence of MTP is independent of $V_{max}^{G6PDH(II)}$. The branch of stable or unstable steady states is indicated with continuous or dashed lines, respectively.

characterized by V_{max}^{G6PDH}. Shown comparatively in Figs. 4 and 5 are the bifurcation analyses as a function of $V_{max}^{G6PDH(II)}$ and V_{max}^{G6PDH}, respectively, at high or low levels of C_P (Figs. 4 and 5) and without MTP (Fig. 5c). With respect to V_{max}^{G6PDH} (from the MTP-independent term of G6PDH rate expression, Eq. 4), the first impression of the model behavior is that control exerted by the branch toward the PP pathway, as compared to the flux through glycolysis (i.e. aldolase; V^{ALD}), is high and negative (notice the slope in Fig. 5a–c). However, the degree of polymerization of MTP modulates the control exerted by the PP branch over the flux through glycolysis. This is evident upon inspection of the model behavior with respect to $V_{max}^{G6PDH(II)}$ (from the MTP-dependent term of G6PDH rate expression, Eq. 4). More specifically, high levels of polymerized MTP (99% of the total pool) drastically reduce the negative control exerted by the PP branch by non-polymerized MTP (55% of the total pool; see Figs. 4 and 6). Metabolite levels are not shown in Fig. 5, but certainly underlie the changes in enzymatic rates through glycolysis and the PP branch. Essentially,

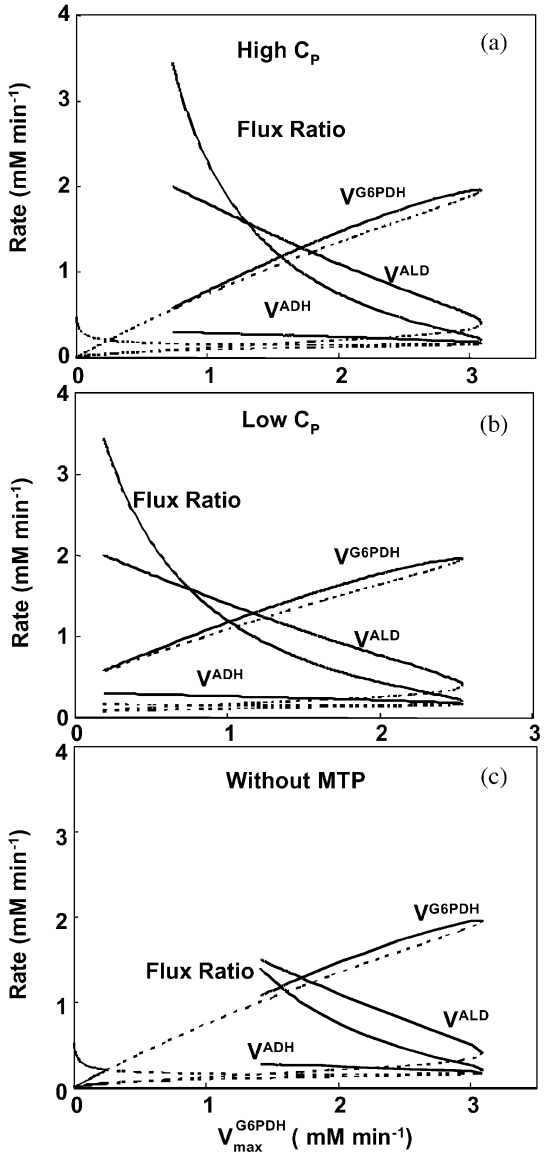

Fig. 5. Stability and bifurcation analyses of the mathematical model as a function of V_{max}^{G6PDH}. The steady state stability and behavior of the mathematical model as well as the existence of bifurcation points were analyzed as a function of V_{max}^{G6PDH} in the presence of (a) high (99% of the total pool of MTP) or (b) low (45% of the total pool of MTP) C_P, or in the absence of MTP (c). For the sake of clarity, the flux ratio of aldolase over the PP pathway, V^{ALD}/V^{G6PDH}, and some fluxes through individual enzymatic steps are depicted. The distinction between branches of stable and unstable steady states is as indicated in Fig. 4.

this is due to the fact that the parameters affecting the rate equations are kept constant except for $V_{max}^{G6PDH(II)}$.

Another important result shows that high (99%) levels of C_P significantly increase the robustness of the metabolic pathway behavior, as can be judged through the stability exhibited by the model over a wide range of variation of $V_{max}^{G6PDH(II)}$ (Fig. 4) when compared with V_{max}^{G6PDH} (Fig. 5) or to the model in the absence of MTP (Fig. 5c). In the case of $V_{max}^{G6PDH(II)}$, an approximate 60-fold increase in the extension of the branch of stable steady states of metabolite concentrations or fluxes through individual enzymatic steps is noted at high (Fig. 4a,b) vs. low C_P (Fig. 4c,d). Remarkably, the model dynamics do not become unstable at high C_P, despite a wide variation in $V_{max}^{G6PDH(II)}$ (Fig. 4a,b); unlike the behavior observed in the presence of low C_P (45%), where limit points are detected (Fig. 4c,d).

The robustness of the metabolic network dynamics and the dependence on the polymerization state of MTP was confirmed by comparing the two main (positive) rate-controlling steps of glycolytic flux, glucose uptake and HK, in the presence or

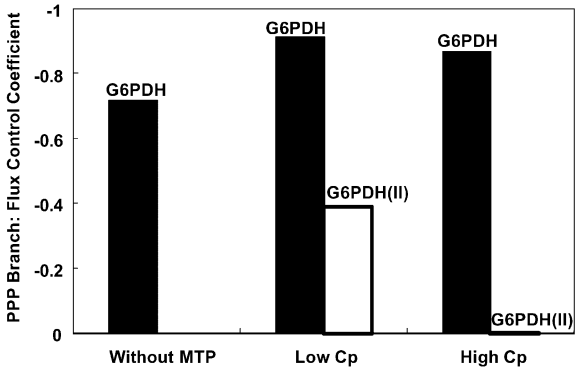

Fig. 6. Flux control analysis obtained from the first derivative of the double logarithmic representation of bifurcation plots. The flux control coefficients of the V_{max}^{G6PDH} (filled columns) and $V_{max}^{G6PDH(II)}$ (empty columns) on the flux through aldolase, V^{ALD} (as a measure of the glycolytic flux), were determined from the slopes of the log–log plot of bifurcation diagrams as a function of V_{max}^{G6PDH} or $V_{max}^{G6PDH(II)}$. In the model without MTP, the contribution by the term containing $V_{max}^{G6PDH(II)}$ in Eq. (4) is null, so is its control coefficient. The set of parameters is as indicated in Table 2 and Fig. 2 for high and low C_P.

absence of MTP. Stable behavior of metabolite concentrations and enzymatic fluxes over the whole metabolic network were obtained over a wide range of variation of the maximal velocities of substrate uptake (V_{max}^{IN}) or conversion by HK (V_{max}^{HK}) (results not shown). When the stability and bifurcation properties of the model at high or low C_P were analyzed as a function of the maximal velocity of PFK (Fig. 7), the highest changes in flux were observed at relatively low V_{max}^{PFK} values under all situations studied. For instance, at high C_P, one expects major changes in the glycolytic flux-controlling properties of the PFK at low V_{max} (given by the slope of V^{ALD} at low V_{max}^{PFK} in Fig. 7a), and indeed, the flux control coefficients for the low range of V_{max}^{PFK} values (0.4–1.0 mM min^{-1}) were in the range of 0.7–0.95, whereas at high V_{max}^{PFK} (=30 mM min^{-1}) the flux control coefficient was only 0.11 (see also Fig. 3). Similar results were obtained for the model behavior in the complete absence of MTP. However, low C_P levels offered a different picture. In the presence of low C_P, the lowest maximal velocity of PFK still congruous with stable behavior was 1.6 mM min^{-1}, whereas in the case of high C_P, the minimal V_{max}^{PFK} value attainable was only 0.4 mM min^{-1}. This is another indication of robustness conferred by high (99%) levels of polymerized MTP.

4. Discussion

The main results obtained in the present work support the notion that the organization and dynamics of assembly–disassembly of microtubular protein may modulate the flux of a metabolic pathway. High levels of polymerized MTP bestow two main properties to the behavior of glycolysis and the branch to the PP pathway, TCA cycle, and ethanolic fermentation (Fig. 1): (i) coherence, as reflected by the coordinated increase or decrease of the glycolytic flux induced by an increase or decrease of polymeric MTP (C_P), respectively (Fig. 2). Essentially, this is explained by the fact that an increase in C_P results in lessening of the (negative) control exerted by the PP pathway on the glycolytic flux, allowing its increase (Figs. 3–6). (ii) Robustness, which is conferred by a significant increase in the range of stable steady state

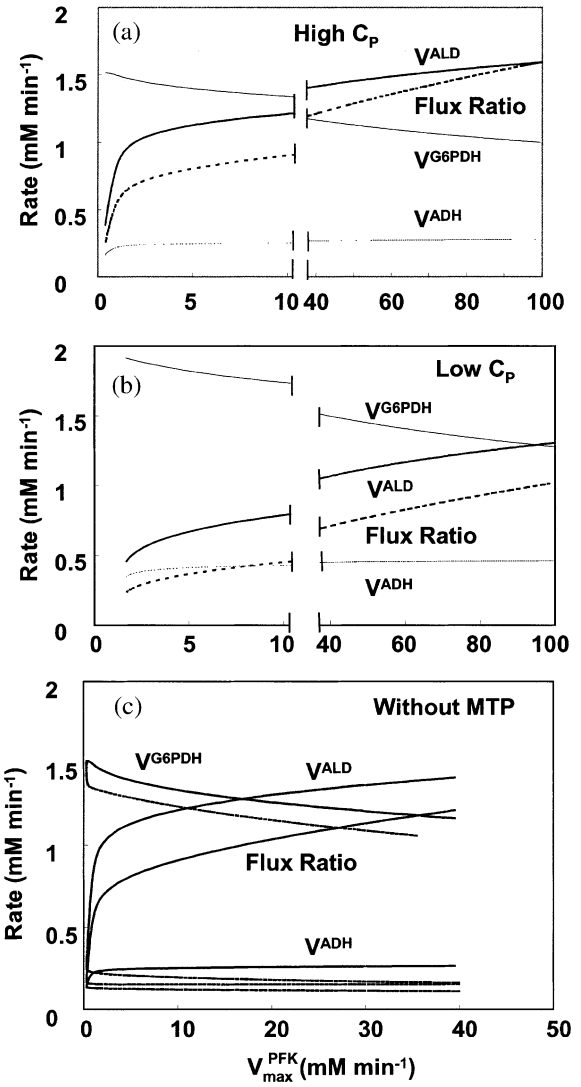

Fig. 7. Stability and bifurcation analyses of the mathematical model as a function of V_{max}^{PFK}. The steady state behavior and stability of the mathematical model as well as the presence of bifurcation points were analyzed as a function of V_{max}^{PFK} in the presence of (a) high (99% of the total pool of MTP) or (b) low (45% of the total pool of MTP) C_P, or in the absence of MTP (c). As in Fig. 5, the flux ratio of glycolysis (i.e. aldolase) over the PP pathway, and some selected fluxes are depicted.

behaviors exhibited by the metabolic network toward variation of, for example, $V_{max}^{G6PDH(II)}$, which catalyzes the branch toward the PP pathway (Fig. 4). Robustness was also evident for the flux-

controlling properties of PFK, which showed an MTP-dependent increase in the range of the lowest maximal velocities attainable by the enzyme (Fig. 7). Such an increase in robustness was induced by high levels of C_P—up to 99% of the total MTP pool. These two properties, coherence and robustness, clearly explain the changes in metabolite concentrations and in the rates of enzymatic steps throughout the metabolic network brought about by MTP polymerization (Fig. 2).

Previous evidence showed that changes in the dynamics of tubulin assembly–disassembly may entrain the dynamics of enzymatic reactions, particularly PK [1,34]. It was also shown that this enzyme may alternate (in a bistable switch) between two oligomeric states (i.e. tetramer–pentamer), in turn entrained by the amount of polymerized MTP and MAPs [1,6,17]. Regardless of the regulatory effects exerted by MTP on PK, this enzyme does not exert control over the glycolytic flux, as deduced by bifurcation and metabolic control analysis. PK only exerts a strong control over the concentration of its substrate, PEP, as evidenced by a high elasticity coefficient (results not shown). In contrast, the finding that when C_P was high, V_{max}^{PFK} could be lowered without introducing instability is in agreement with enhanced robustness conferred by the microtubular cytoskeleton (Fig. 7). This is a very important trait since an increase in robustness may allow some nodes of the metabolic network, e.g. PFK, to retain their flux-controlling attributes despite drastic changes in metabolic conditions (Fig. 7; see also text).

The steady state flux of glycolysis, as a function of the depolymerization constant k_{dp}, increased with the level of polymerized MTP (Fig. 2c). Glycolytic flux increased from 1.95 mM min^{-1} at 33% polymeric MTP, to 2.73 mM min^{-1} at 99% polymerized MTP; a 40% increase (Fig. 2c). A smaller increase was obtained when the polymerization constant, k_{pol}, was analyzed (a 13% increase; Fig. 2c, inset).

The values of glucose uptake rates used in the model simulations are of the same order of magnitude of those determined in aerobic, glucose-limited chemostat cultures of yeast [30,32]. When yeast cells actively divide, microtubules attain their maximal degree of polymerization [40,41]. Fast growing yeast cells spend most of their time in the S, G2 and M phases of the cell division cycle as determined by flow cytometry in chemostat cultures [31]. In rapidly dividing cells, microtubules are, on average, more polymerized than in the G1 phase of the cell cycle [40,41]. We found that the time yeast cells spend in G1 phase decreases exponentially with the growth rate [42], and this is coincident with a change in slope of the glucose uptake rate [31,32] (see Fig. 2c). Taken together, these results point out that the glycolytic flux correlates with the polymerization state of the microtubules, which can be indirectly judged by the percentage of yeast cells undergoing active division.

The stability analysis at low and high C_P shows that, as a function of $V_{max}^{G6PDH(II)}$, the metabolic network bifurcates at limit points only when there are reduced levels of polymerized MTP ($\sim$45%) (Fig. 4). This observation suggests that the extent of cytoskeleton polymerization in cells could be regulated so as to achieve stable behavior under challenging environmental conditions. After such limit points, we were not able to find a stable branch of steady states (see, e.g. Figs. 2, 4 and 5); in other words, the network did not reveal multiple stationary states. In this state, we would expect that some other parameters would have to change or new reactions or mechanisms would activate for the system to remain stable, a topic that needs further investigation.

In summary, cytoskeletal organization induces coherent behavior in a metabolic network at the level of control of the flux partition between glycolysis and the PP pathway. Additionally, high levels of polymerized MTP increase the robustness of the metabolic network's steady state dynamics. These properties add to the plasticity of mass-energy transforming networks to adapt to changing environmental conditions without losing stability while retaining biological function.

Acknowledgments

M.A. Aon and S. Cortassa are researchers from CONICET, Argentina. We gratefully acknowledge Prof. B. O'Rourke and Prof. R.L. Winslow (Johns

Hopkins University, School of Medicine) for critical comments and suggestions on the manuscript.

References

[1] M.A. Aon, S. Cortassa, Dynamic Biological Organization. Fundamentals as Applied to Cellular Systems, Chapman and Hall, London, 1997.
[2] M.A. Aon, S. Cortassa, D.F. Gomez Casati, A.A. Iglesias, Effects of stress on cellular infrastructure and metabolic organization in plant cells, Int. Rev. Cytol. 194 (2000) 239–273.
[3] M.A. Aon, S. Cortassa, D. Lloyd, Fractal space and chaotic dynamics in biochemistry: simplicity underlies complexity, Cell Biol. Int. 24 (2000) 581–587.
[4] J. Ovádi, P.A. Srere, Macromolecular compartmentation and channeling, Int. Rev. Cytol. 192 (2000) 255–280.
[5] B.G. Vértessy, F. Orosz, J. Kovács, J. Ovadi, Alternative binding of two sequential glycolytic enzymes to microtubules, J. Biol. Chem. 272 (1997) 25542–25546.
[6] S. Cortassa, A. Cáceres, M.A. Aon, Microtubular protein in its polymerized or non-polymerized states differentially modulates in vitro and intracellular fluxes catalyzed by enzymes related to carbon metabolism, J. Cell. Biochem. 55 (1994) 120–132.
[7] M.A. Aon, A. Cáceres, S. Cortassa, Heterogeneous distribution and organization of cytoskeletal proteins drive differential modulation of metabolic fluxes, J. Cell. Biochem. 60 (1996) 271–278.
[8] D. Haussinger, F. Lang, W. Gerok, Regulation of cell function by the cellular hydration state, Am. J. Physiol. 30 (1994) E343–E355.
[9] J.C. Parker, In defense of cell volume?, Am. J. Physiol. 265 (1993) C1191–C1200.
[10] P.R. Cook, The nucleoskeleton and the topology of transcription, Eur. J. Biochem. 185 (1989) 487–501.
[11] P.R. Cook, The nucleoskeleton and the topology of replication, Cell 66 (1991) 627–635.
[12] S. Grabski, X.G. Xie, J.F. Holland, M. Schindler, Lipids trigger changes in the elasticity of the cytoskeleton in plant cells: a cell optical displacement assay for live cell measurements, J. Cell Biol. 126 (1994) 713–716.
[13] G.G. Gundersen, T.A. Cook, Microtubules and signal transduction, Curr. Op. Cell Biol. 11 (1999) 81–94.
[14] D.F. Alonso, H.G. Farina, C. Arregui, M.A. Aon, D.E. Gomez, Modulation of urokinase-type plasminogen activator and metalloproteinase activities in cultured mouse mammary-carcinoma cells: enhancement by paclitaxel and inhibition by nocodazole, Int. J. Cancer 83 (1999) 242–246.
[15] D. Haussinger, B. Stoll, S. vom Dahl, et al., Effect of hepatocyte swelling on microtubule stability and tubulin mRNA levels, Biochem. Cell Biol. 72 (1994) 12–19.
[16] P. Marmillot, T. Keith, D.K. Srivastava, H.R. Knull, Effect of tubulin on the activity of the muscle isoenzyme of lactate dehydrogenase, Arch. Biochem. Biophys. 315 (1994) 467–472.
[17] M.A. Aon, S. Cortassa, A. Cáceres, Computation in cellular and molecular biological systems, in: R. Cuthbertson, M. Holcombe, R. Paton (Eds.), Models of Cytoplasmic Structure and Function, World Scientific, London, 1996, p. 195.
[18] K. Liliom, G. Wágner, J. Kovács, et al., Combined enhancement of microtubule assembly and glucose metabolism in neuronal systems in vitro: decreased sensitivity to copper toxicity, Biochim. Biophys. Res. Commun. 264 (1999) 605–610.
[19] M.A. Aon, D.F. Gomez-Casati, A.A. Iglesias, S. Cortassa, Ultrasensitivity in (supra)molecularly organized and crowded environments, Cell Biol. Int. 25 (2001) 1091–1099.
[20] K. Luby-Phelps, Cytoarchitecture and physical properties of cytoplasm: volume, viscosity, diffusion, intracellular surface area, Int. Rev. Cytol. 192 (2000) 189–221.
[21] M.A. Lutherand, J.C. Lee, The role of phosphorylation in the interaction of rabbit muscle phosphofructokinase with F-actin, J. Biol. Chem. 261 (1986) 1753–1759.
[22] B. Pedrotti, L. Ulloa, J. Avila, K. Islam, Characterization of microtubule-associated protein MAP1B: phosphorylation state, light chains, and binding to microtubules, Biochemistry 35 (1996) 3016–3023.
[23] S.J. Roberts, G.N. Somero, Binding of phosphofructokinase to filamentous actin, Biochemistry 26 (1987) 3437–3442.
[24] H.R. Knull, J.L. Walsh, Association of glycolytic enzymes with the cytoskeleton, Curr. Top. Cell. Regul. 33 (1992) 15–30.
[25] G. Minascheck, U. Groschel-Stewart, S. Blumand, J. Bereither-Hahn, Microcompartmentation of glycolytic enzymes in cultured cells, Eur. J. Cell Biol. 58 (1992) 418–428.
[26] R. Karkhoff-Schweizerand, H.R. Knull, Demonstration of tubulin–glycolytic enzyme interactions using a novel electrophoretic approach, Biochem. Biophys. Res. Commun. 146 (1987) 827–831.
[27] S. Cortassa, J.C. Aon, M.A. Aon, Fluxes of carbon, phosphorylation, and redox intermediates during growth of *Saccharomyces cerevisiae* on different carbon sources, Biotech. Bioeng. 47 (1995) 193–208.
[28] M.A. Aon, M.E. Mónaco, S. Cortassa, Carbon and energetic uncoupling are associated with block of division at different stages of the cell cycle in several cdc mutants of *Saccharomyces cerevisiae*, Exp. Cell Res. 217 (1995) 42–51.
[29] S. Cortassa, M.A. Aon, Metabolic control analysis of glycolysis and branching to ethanol production in chemostat cultures of *Saccharomyces cerevisiae* under carbon, nitrogen, or phosphate limitations, Enz. Microb. Technol. 16 (1994) 761–770.
[30] S. Cortassa, M.A. Aon, Distributed control of the glycolytic flux in wild-type cells and catabolite repression mutants of *Saccharomyces cerevisiae* growing in carbon-limited chemostat cultures, Enz. Microb. Technol. 21 (1997) 596–602.

[31] M.A. Aon, S. Cortassa, Catabolite repression mutants of *Saccharomyces cerevisiae* show altered fermentative metabolism as well as cell cycle behavior in glucose-limited chemostat cultures, Biotech. Bioeng. 59 (1998) 203–213.

[32] S. Cortassa, M.A. Aon, The onset of fermentative metabolism in continuous cultures depends on the catabolite repression properties of *Saccharomyces cerevisiae*, Enz. Microb. Technol. 22 (1998) 705–712.

[33] M.F. Carlier, R. Melki, D. Pantaloni, T.L. Hill, Y. Chen, Synchronous oscillations in microtubule polymerization, Proc. Natl. Acad. Sci. USA 84 (1987) 5257–5261.

[34] S. Cortassa, M.A. Aon, Biothermokinetics of the living cell, in: H.V. Westerhoff, J. Snoep (Eds.), Entrainment of Enzymatic Activity by the Dynamics of Cytoskeleton, Biothermokinetics, Amsterdam, 1996, p. 337.

[35] H.M. Sauro, J.R. Small, D.A. Fell, Metabolic control and its analysis. Extensions to the theory and matrix method, Eur. J. Biochem. 165 (1987) 215–221.

[36] H.V. Westerhoff, D.B. Kell, Matrix method for determining steps most rate-limiting to metabolic fluxes in biotechnological processes, Biotech. Bioeng. 30 (1987) 101–107.

[37] R.H. Abraham, Self-organising systems. The emergence of order, in: F.E. Yates, A. Garfinkel, D.O. Walter, G.B. Yates (Eds.), Dynamics and Self-Organisation, Plenum Press, New York, 1987, p. 599.

[38] M. Kubicek, M. Marek, Computational Methods in Bifurcation Theory and Dissipative Structures, Springer Verlag, New York, 1983.

[39] E. Doedle, AUTO Manual, California Institute of Technology, Pasadena, 1986.

[40] M.D. Welch, D.A. Holtzman, D.G. Drubin, The yeast actin cytoskeleton, Curr. Op. Cell Biol. 6 (1994) 110–119.

[41] J. Chant, Cell polarity in yeast, TIG 10 (1994) 328–333.

[42] M.A. Aon, S. Cortassa, Quantitation of the effects of disruption of catabolite (de)repression genes on the cell cycle behavior of *Saccharomyces cerevisiae*, Curr. Microbiol. 38 (1999) 57–60.

[43] M. Rizzi, U. Theobald, E. Querfurth, T. Rohrhirsch, M. Baltes, M. Reuss, In vivo investigations of glucose transport in *Saccharomyces cerevisiae*, Biotech. Bioeng. 49 (1996) 316–327.

[44] J.L. Galazzo, J.E. Bailey, Fermentation pathway kinetics and metabolic flux control in suspended and immobilized *Saccharomyces cerevisiae*, Enz. Microb. Technol. 12 (1990) 162–172.

[45] J. Monod, J. Wyman, J.P. Changeux, On the nature of allosteric transitions: a plausible model, J. Mol. Biol. 12 (1965) 88–118.

[46] B. Hess, T. Plesser, Temporal and spatial order in biochemical systems, Ann. NY Acad. Sci. 316 (1978) 203–213.